nature chemistry

ARTICLES

PUBLISHED ONLINE: 26 SEPTEMBER 2016 | DOI: 10.1038/NCHEM.2615

An infrared spectroscopy approach to follow β-sheet formation in peptide amyloid assemblies

Jongcheol Seo[1†], Waldemar Hoffmann[1,2†], Stephan Warnke[1], Xing Huang[1], Sandy Gewinner[1], Wieland Schöllkopf[1], Michael T. Bowers[3], Gert von Helden[1*] and Kevin Pagel[1,2*]

Amyloidogenic peptides and proteins play a crucial role in a variety of neurodegenerative disorders such as Alzheimer's and Parkinson's disease. These proteins undergo a spontaneous transition from a soluble, often partially folded form, into insoluble amyloid fibrils that are rich in β-sheets. Increasing evidence suggests that highly dynamic, polydisperse folding intermediates, which occur during fibril formation, are the toxic species in the amyloid-related diseases. Traditional condensed-phase methods are of limited use for characterizing these states because they typically only provide ensemble averages rather than information about individual oligomers. Here we report the first direct secondary-structure analysis of individual amyloid intermediates using a combination of ion mobility spectrometry–mass spectrometry and gas-phase infrared spectroscopy. Our data reveal that oligomers of the fibril-forming peptide segments VEALYL and YVEALL, which consist of 4–9 peptide strands, can contain a significant amount of β-sheet. In addition, our data show that the more-extended variants of each oligomer generally exhibit increased β-sheet content.

The assembly of peptides and proteins into insoluble β-sheet-rich fibrils is a common hallmark of all amyloid diseases[1–3]. In the disease case, however, small soluble oligomers rather than mature fibrils have been suggested as the toxic species. Oligomers of amyloidogenic peptides, such as the β-amyloid peptide[4–6], α-synuclein[7], islet amyloid polypeptide[8,9], insulin[10,11] and several others, are suspected to be responsible for Alzheimer's, Parkinson's, type II diabetes and so on. Exploring the structure of these oligomers is not only crucial to develop a better understanding of the underlying molecular details of amyloid assembly, but it is also key to the development of novel diagnostic and therapeutic methods.

Extensive structural studies using X-ray diffraction, nuclear magnetic resonance spectroscopy and electron microscopy (EM) have revealed that highly ordered β-sheets maintained by cross-β spines are dominant in mature fibrils[11–15]. Moreover, circular dichroism and infrared spectroscopy studies revealed that large secondary structural transitions from partially helical or unordered structures into repeating β-sheets occur during the assembly process[16–18]. Thus, to determine the secondary structure of pre-fibrillar oligomers and identify the specific states responsible for the secondary structural transitions to a β-sheet should be the first step in investigating the assembly of amyloid peptides and proteins. However, the polydisperse, polymorph, and transient nature of the involved oligomers makes structural investigations inherently challenging, because oligomers usually exist in a distribution of distinct stoichiometries and conformational states. Traditional condensed-phase methods are of limited use for structural studies of these systems because they only yield ensemble-averaged results. Thus, several methods based on mass spectrometry (MS) and ion mobility spectrometry (IMS) have been applied to study amyloid assembly[19–28]. With its unique capability to isolate and detect molecular ions of a specific mass-to-charge ratio (m/z) and to measure collision cross-sections (CCSs), recent IMS–MS studies successfully isolated size- and shape-specific oligomer states of amyloidogenic peptides and extracted structural as well as oligomer distribution information.

The peptide VEALYL, which corresponds to segment 12–17 of the insulin B chain, was recently shown to form amyloid fibrils that later evolve into microcrystals in solution[14,15,20]. X-ray studies have revealed that the peptides assemble into a so-called steric zipper—a repeating pattern of antiparallel β-sheets with densely packed, interdigitated side chains[12,14,15]. IMS–MS methods found that a structural transition from a compact to a more-extended structure appears early in the assembly process[20]. However, IMS–MS is not sensitive to the secondary structure itself; it only gives information about the overall shape of a molecule and relies on comparison with modelling studies to obtain structural information.

To address this limitation, we combined infrared spectroscopy with IMS–MS to probe the structure of shape- and m/z-selected ions. Infrared spectroscopy is a versatile tool for identifying secondary structures[29,30]. The stretching mode of C=O groups (amide I) in the peptide backbone can be especially diagnostic for different types of secondary structure. Highly ordered structures, such as α-helices and β-sheets, yield major amide I bands at 1,650–1,660 cm^{-1} and 1,610–1,640 cm^{-1}, respectively[29]. Random coils and several turn structures, on the other hand, yield amide I features at 1,640–1,650 cm^{-1} and 1,660–1,685 cm^{-1}, respectively, which are both distinct from those of β-sheets[29,30]. Recent advances in laser-based methods enable us to record infrared spectra of m/z- and/or ion-mobility-selected molecular ions[31,32]. Irradiating the isolated molecular ions with an intense tunable infrared laser can lead to the absorption of multiple infrared photons and subsequent dissociation. Plotting the fragmentation yield as a function of infrared wavelength gives a gas-phase infrared multiple-photon dissociation (IRMPD) spectrum, which resembles the condensed-phase infrared absorption spectrum. In the present work we investigated oligomers of VEALYL and its sequence-scrambled peptides, VELYAL and YVEALL, using these techniques.

[1]Fritz-Haber-Institut der Max-Planck-Gesellschaft, Faradayweg 4-6, Berlin 14195, Germany. [2]Institute of Chemistry and Biochemistry, Freie Universität Berlin, Takustrasse 3, Berlin 14195, Germany. [3]Department of Chemistry and Biochemistry, University of California Santa Barbara, Santa Barbara, California 93106, USA. †These authors contributed equally to this work. *e-mail: helden@fhi-berlin.mpg.de; kevin.pagel@fu-berlin.de

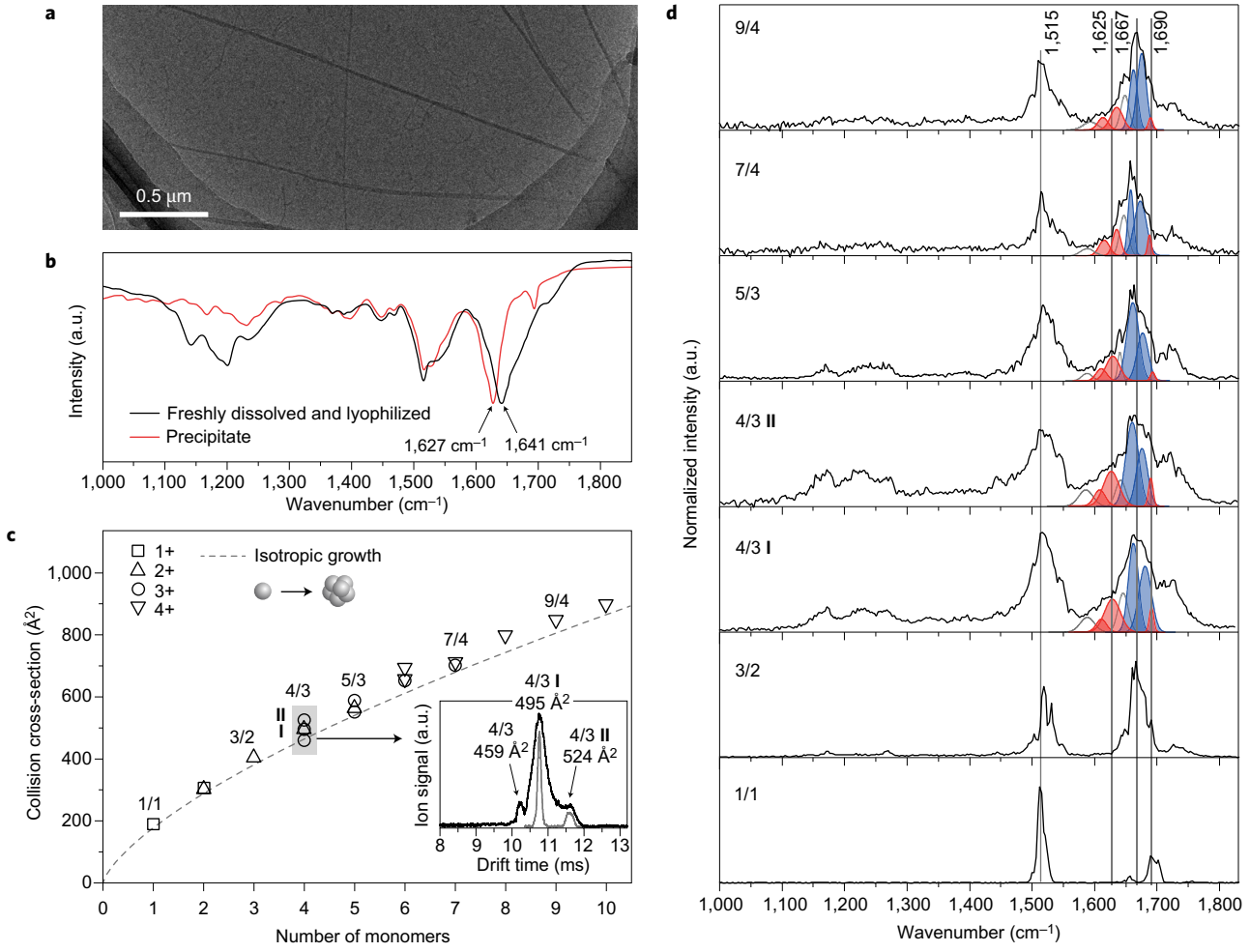

Figure 1 | Structural analysis of VEALYL oligomers and fibrils in the condensed phase and in the gas phase. a, TEM of an incubated VEALYL solution. **b**, Solid FTIR spectra of the VEALYL precipitate obtained after two days of incubation at room temperature and of the freshly dissolved VEALYL without precipitation after lyophilization. **c**, Measured CCSs of VEALYL oligomers as a function of the number of monomers. The dashed line denotes the expected CCSs assuming isotropic growth. The inset shows a typical ATD of the triply charged tetramer (4/3) in which multiple conformers with distinct CCSs are observed. The statistical error of the CCS measurements is less than 1% and smaller than the size of the symbols. **d**, IRMPD spectra of *m/z*- and drift-time-selected VEALYL oligomer ions from the singly protonated monomer (1/1) up to the quadruply protonated nonamer (9/4) measured in the wavenumber range 1,000–1,850 cm^{-1}. Fractions of the amide I band that are representative for β-sheets (1,610–1,640 cm^{-1} and 1,690 cm^{-1}) and turn-like (1,660–1,685 cm^{-1}) structures are represented in red and blue, respectively. For details about the fitting procedure see Supplementary Information.

Results and discussion

The hexapeptide VEALYL is well known to form amyloid fibrils[11,12,14,15]. This manifests itself in the formation of an insoluble deposition after the incubation of VEALYL in water/methanol at room temperature. Figure 1a shows a transmission electron micrograph of amyloid fibrils that are formed from the VEALYL sample. The secondary structure of non-soluble VEALYL fibrils was previously found to be dominated by β-sheets[11–15]. Solid-state Fourier transform infrared (FTIR) spectroscopy, especially in the amide I region where C=O vibrations are probed, is sensitive to the secondary structure. Highly ordered antiparallel β-sheets are expected to yield amide I bands at 1,610–1,640 cm^{-1} and ~1,690 cm^{-1}, whereas signals at 1,640–1,650 cm^{-1} and 1,660–1,685 cm^{-1} indicate random coils and several types of turn structures, respectively[29,30]. A comparison between FTIR spectra of freshly dissolved VEALYL and the precipitate is shown in Fig. 1b. For the freshly dissolved sample (black curve), the maximum of the amide I band at 1,641 cm^{-1} together with several broad features up to 1,700 cm^{-1} indicate the presence of unordered and turn-like structures. In contrast, the infrared spectrum of the VEALYL precipitate (red curve) shows a narrower and red-shifted amide I band centred at ~1,627 cm^{-1}. This suggests that the VEALYL precipitate predominantly consists of highly ordered β-sheets. In addition, ultraviolet spectroscopy and FTIR experiments in solution (Supplementary Fig. 4) show that aggregation occurs after a certain lag phase, which is characteristic for nucleation-dependent fibril formation[33].

A disadvantage of condensed-phase methods is that in solution they can only provide ensemble-averaged results of all the aggregation states. Structural details of the individual pre-fibrillar oligomers are, thus, impossible to obtain with these methods. To address this limitation, IMS–MS-based methods were used in the present work. These methods allow a clear separation of the oligomer number (n) and conformation, as well as provide absolute CCSs. When a freshly dissolved VEALYL sample is electrosprayed, a wide distribution of multiply charged peptide oligomers is observed (Supplementary Figs 5 and 6). The CCS values of each individual VEALYL conformer were measured and the results are shown in Fig. 1c. The dashed line represents an ideal isotropic (that is, globular) growth behaviour following $\sigma = \sigma_1 n^{2/3}$, where σ_1 denotes the CCS of the monomer[20]. This CCS plot clearly shows the polydisperse and polymorph nature of VEALYL oligomers, and features oligomers with various stoichiometries that range from the singly protonated monomer

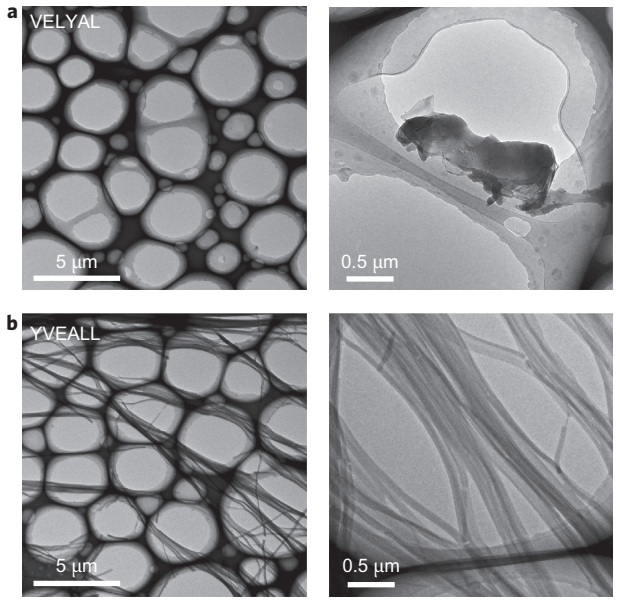

Figure 2 | TEM images of VEALYL sequence variants. a,**b**, VELYAL (**a**) and YVEALL (**b**) images were obtained after incubation at room temperature for 29 days and subsequent evaporation of the solvent. For VELYAL, only the TEM grid was observed with no fibrils, whereas fibril formation was observed for YVEALL.

($n/z = 1/1$) to the quadruply protonated decamer ($n/z = 10/4$). The inset in Fig. 1c shows an arrival-time distribution (ATD) of the triply protonated tetramer ($n/z = 4/3$) for which multiple species with different CCSs were observed. Interestingly, VEALYL oligomers larger than the trimer ($n > 3$) exhibit CCS values that are larger than predicted by the isotropic model. This deviation from the isotropic growth line may be indicative of the presence of soluble β-sheet-rich intermediates on the way to fibril formation, as suggested by previous studies[14,20].

Although ion-mobility data contain information about the overall size of oligomer ions, they cannot provide clear evidence for a specific secondary structure. To obtain information about the structural details of individual oligomers, the IMS–MS instrument was used as a preparative tool to pre-select ions of a specific size and m/z, followed by irradiation with intense infrared laser pulses generated by the Fritz Haber Institute free-electron laser (FHI-FEL)[34]. An IRMPD spectrum can then be generated from the wavelength-dependent dissociation of the pre-selected ions. The resulting IRMPD spectra of individual VEALYL oligomers up to the quadruply protonated nonamer ($n/z = 9/4$) measured in a wavenumber range of 1,000–1,850 cm^{-1} are shown in Fig. 1d. The spectra consist of two major bands at 1,600–1,700 cm^{-1} and 1,450–1,550 cm^{-1}, which can be assigned as amide I and II vibrations, respectively. Infrared features above 1,700 cm^{-1} originate from carboxylic acid vibrations either from the C terminus or from the side chain of glutamic acid. Weaker features in the wavenumber range 1,100–1,300 cm^{-1} can be assigned to Tyr and amide III vibrations[30,35]. For the singly protonated monomer ($n/z = 1/1$), well-separated features can be observed in the amide I region at 1,655 and 1,695–1,705 cm^{-1}, as well as a very weak feature at 1,750 cm^{-1}. Compared with the amide I bands of higher oligomers, these monomer features are found at higher wavenumbers. This is not surprising because the extent of hydrogen bonding inside the hexapeptide monomer is expected to be rather low and, thus, provide little perturbation of the individual C=O oscillators. As the size of the oligomer increases, amide I features are shifted towards lower wavenumbers. The spectra of higher oligomers ($n = 3$–9) feature amide I bands that are centred around 1,660–1,670 cm^{-1}, which is indicative of turn-like structures. Most interesting, however, is the observation of typical β-sheet infrared bands in the amide I region (1,610–1,640 cm^{-1}) for the tetramer and higher oligomers, which clearly have larger CCSs than predicted by the isotropic growth model. To ascertain qualitatively the relative abundances of β-sheets and turn-like structures, the amide I region (1,600–1,700 cm^{-1}) of these oligomers ($n = 4$–9) was fitted with multiple Gaussian curves (Fig. 1d (for details see Supplementary Fig. 7 and Supplementary Table 5)). Each of these Gaussians represents a specific motif: β-sheets at 1,610–1,640 cm^{-1} and ~1,690 cm^{-1} (Fig. 1d, red curve) and small turns at 1,660–1,685 cm^{-1} (blue curve). This analysis clearly indicates a significant proportion of β-sheets in the higher VEALYL oligomers of $n \geq 4$.

Compared with the clear evidence for β-sheets in the solid FTIR spectra of the mature VEALYL fibrils (Fig. 1b), however, β-sheet signatures in the IRMPD spectra of VEALYL oligomers (Fig. 1d) are weaker and exhibit little variation over the different oligomer sizes. This makes it difficult to correlate the IRMPD results with the observed CCSs and to pinpoint specific oligomers that are involved in structural transitions. To generate comparable peptides that may differ in their amyloid-formation propensity, the VEALYL-sequence variants VELYAL and YVEALL were synthesized and investigated. Keeping the overall amino acid composition unchanged helps to minimize differences in the infrared spectra that arise from different amino acid side-chain absorptions and greatly facilitates the comparison between different sets of infrared data.

As shown in the TEM image in Fig. 2a, VELYAL does not appear to form amyloid fibrils. Similarly, no visible precipitate was formed after several days of incubation, which was further confirmed by ultraviolet spectroscopy. Time-resolved FTIR measurement of a VELYAL solution did not indicate a structural transition into β-sheets (Supplementary Fig. 8). Similarly, the solid-phase FTIR spectra of fresh and incubated VELYAL samples both exhibit an amide I peak at 1,638 cm^{-1} and broad features up to 1,750 cm^{-1}, which indicates that mostly unordered structures are present and no β-sheets are formed (Supplementary Fig. 9). Taken together, these results show that VELYAL is a non-amyloid-forming sequence, which makes it an ideal reference for further comparison. VELYAL does form oligomers that can be investigated further by IMS–MS and IRMPD (Supplementary Figs 10–13). However, their CSSs more closely follow the isotropic growth curve than those of either of the other two peptides, which indicates a compact and rather globular set of conformations (Supplementary Figs 11 and 12). In addition, the IRMPD spectra show almost no sign of β-sheet formation and point to a predominantly unordered or turn-like conformation (Supplementary Fig. 13 and Supplementary Table 7). These results emphasize that the increased β-sheet content observed for VEALYL is a real effect and not just an artefact of the IRMPD measurements.

In stark contrast to the non-amyloidogenic variant VELYAL, the TEM micrographs of YVEALL clearly point to the formation of amyloid fibrils (Fig. 2b). This is further supported by the FTIR spectra of the lyophilized precipitate, which exhibit a sharp infrared band at 1,627 cm^{-1}, indicating the presence of highly ordered β-sheets (Supplementary Fig. 14). In addition, time-dependent ultraviolet spectroscopy and solution-phase FTIR experiments (Supplementary Fig. 15) of YVEALL reveal a typical nucleation-dependent fibril growth, which is, however, slower than that of the original sequence VEALYL. This makes YVEALL an ideal candidate for the spectroscopic investigation of intermediate amyloid oligomers.

In IMS–MS a wide distribution of oligomers of different size and charge is observed for YVEALL (Supplementary Figs 16 and 17). The CCS evolution of different oligomers as a function of the oligomer number n is shown in Fig. 3a. For species up to the tetramer ($n = 1$–4), only little deviation from the isotropic growth model (dashed line) is observed. Larger oligomers ($n > 4$), however,

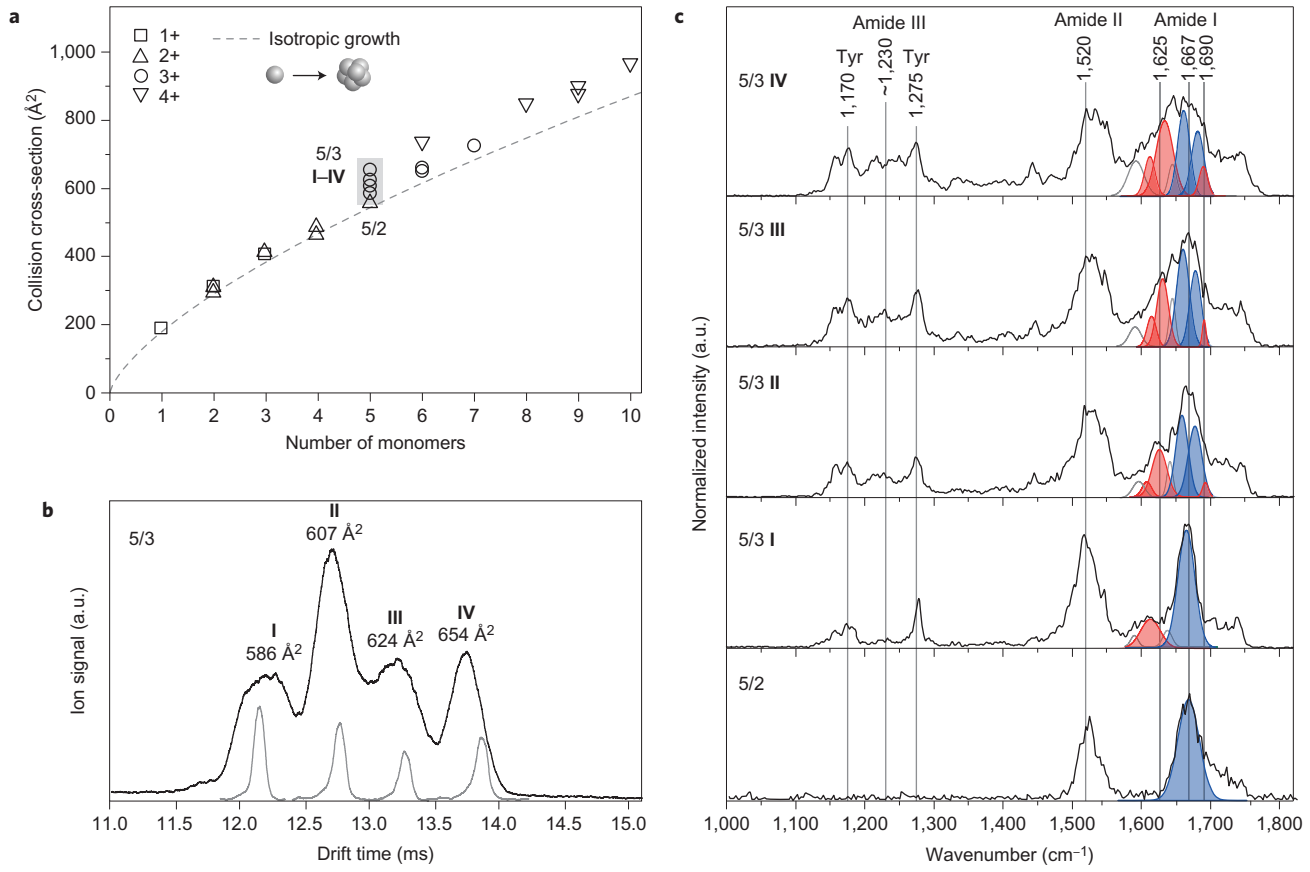

Figure 3 | IMS and conformer-selected infrared spectroscopy of YVEALL oligomers. a, CCSs of YVEALL oligomers as a function of the number of monomers. The dashed line denotes isotropic growth. The statistical error of the measured CCSs is less than 1% and smaller than the symbol size. **b**, An ATD of the triply protonated pentamer (5/3) for which multiple conformers with distinct CCSs are observed. The narrow peaks depicted in grey correspond to the portions of the oligomer distribution that were selected for further IRMPD-spectroscopic analysis. a.u., arbitrary units. **c**, IRMPD spectra of the doubly protonated pentamer (5/2) and the drift-time-selected species (**I**–**IV**) of the triply protonated YVEALL pentamers (5/3). The amide I region (1,600–1,700 cm^{-1}) was fitted by multiple Gaussian peaks. The blue and red Gaussians represent infrared bands that correspond to turn-like (1,660–1,685 cm^{-1}) and β-sheet (1,610–1,640 cm^{-1} and ~1,690 cm^{-1}) structures, respectively. Details of the fitting procedure are given in Supplementary Information.

exhibit significantly higher CCSs than predicted by the isotropic model. Figure 3b shows an ATD of the triply protonated pentamers (5/3), for which at least four distinct conformers can be separated (labelled **I**–**IV**). The smallest observed pentamer (5/2) fits to the isotropic model, whereas the largest pentamer (5/3, **IV**) is ~23% larger in CCS compared with isotropic oligomers. YVEALL pentamers are therefore highly polymorph and represent a transition from globular species close to the isotropic line to much more extended states.

The IRMPD spectra of each 5/3 conformer are given in Fig. 3c. All the spectra show strong amide II and I features in the 1,500–1,580 cm^{-1} and 1,600–1,700 cm^{-1} region, respectively, and additionally exhibit pronounced signals at 1,100–1,300 cm^{-1}, which correspond to Tyr and amide III vibrations. It is interesting to observe how the individual infrared bands change when the pentamers become more extended. The amide II band only undergoes a small blueshift and broadening as the CCS increases. This is not surprising because the amide II band consists of N–H and C–N bending modes, which are only marginally affected by changes in the secondary structure[24]. The diagnostic amide I band, however, shows a strong variation between different pentamers. For the doubly protonated pentamer (5/2), the amide I modes are centred at 1,667 cm^{-1} and do not exhibit IRMPD features in the typical β-sheet range between 1,610 and 1,640 cm^{-1}. However, as the cross-sections of the polymorph pentamers increase (from species **I** to **IV**), typical β-sheet amide I features at 1,610–1,640 cm^{-1} and 1,690 cm^{-1} make up a considerable fraction of the overall spectrum. To allow a more-quantitative assessment, the infrared traces of the individual pentamers (**I**–**IV**) were fitted in the amide I region by multiple Gaussians, as shown in Fig. 3c (details are given in Supplementary Table 9). The curves in red represent the characteristic β-sheet bands and the curves in blue correspond to turn-like features. Clearly, the β-sheet bands increase as the CCS increases. The most extended pentamer, **IV**, exhibits a significant amount of IRMPD features at 1,610–1,640 cm^{-1} and 1,690 cm^{-1} that are characteristic for the existence of antiparallel β-sheet structures. For further illustration of the increased β-sheet content, difference spectra are shown in Supplementary Fig. 18.

Additional support for a possible transition in the secondary structure is provided by the increasing intensities of the infrared bands at around 1,220–1,240 cm^{-1} for conformations with increasing CCS. These bands can be tentatively assigned to amide III bands typical for antiparallel β-sheets[30,35]. Additional structural information can be drawn from amino acid side-chain vibrations. According to X-ray crystallography studies, half of all the amino acid side chains in amyloid fibrils only weakly interact with other side chains or the peptide backbone. For globular oligomers, on the other hand, extensive interactions between side chains or with the backbone are essential to maintain the compact structure[11,14]. These characteristics are also reflected in the IRMPD spectra of the corresponding structures, and lead to signatures of free side chains for fibril-like species and less-pronounced features for globular types. This behaviour is revealed in the spectra of the polymorph YVEALL pentamers in

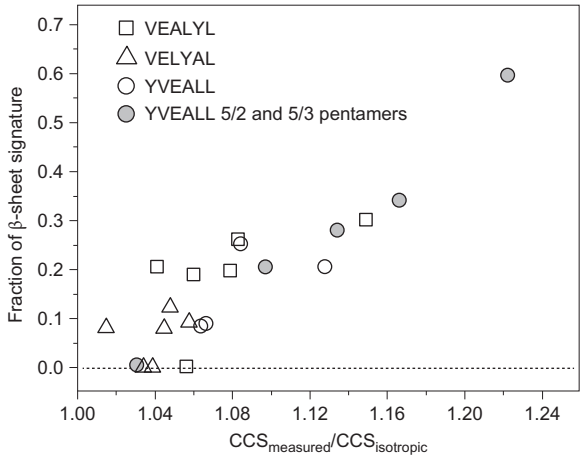

Figure 4 | Correlation between increase in CCS and β-sheet fraction. Fraction of β-sheet in the amide I band of VEALYL, VELYAL and YVEALL oligomers as a function of relative deviation in CCS from the isotropic growth model. Shaded circles denote the polymorph pentamers (5/2 and 5/3, **I**–**IV**) of YVEALL, which are discussed in detail in Fig. 3.

Fig. 3c. Infrared bands that can be assigned to C–O–H bending (1,170 cm^{-1}) and C–OH stretching (1,275 cm^{-1}) vibrations of free tyrosine residues[30], as well as signals at 1,700–1,750 cm^{-1} that correspond to C=O stretching vibrations of weakly bound carboxylic acids, can all be identified with increasing intensities for species with increasing cross-section. Taken together, the presented results from IMS–MS and IRMPD spectroscopic experiments strongly suggest that pentamers of the fibril-forming sequence YVEALL are soluble early intermediates that undergo secondary structural transitions from a compact unordered structure to an extended assembly of repeating β-sheets.

As shown in Supplementary Fig. 19, larger YVEALL oligomers (7/3 and 9/4) show considerable β-sheet features, but they are less pronounced compared with the most-extended pentamer (5/3 **IV**). Thus, the oligomer number does not correlate directly with an increased β-sheet character. This suggests that the formation of larger oligomers is not necessarily initiated by the most-extended pentamer. The complex equilibrium between different oligomeric states is established during the early stages of aggregation—the lag phase—and thus a multitude of oligomers with distinct β-sheet content coexist.

Oligomers rich in β-sheet structure have larger CCSs than globular conformations (isotropic line). Hence, the deviation in CCSs from the isotropic growth model, which is similar to a shape factor[36–38] that describes the structural anisotropy in proteins, more probably correlates with the relative β-sheet character than the oligomer size[20]. Thus, we calculated the fraction of β-sheet signature within the amide I band in all the investigated species by dividing the summed area of β-sheet features in the IRMPD spectra (red curves) by the total area of the amide I band (Supplementary Tables 6, 8 and 10). The result is shown in Fig. 4. Oligomers of VELYAL barely deviate from the isotropic line (less than 5%) and feature β-sheet signatures that make up less than 10% of the total amide I band. The amyloid-forming sequences VEALYL and YVEALL, on the other hand, show more-pronounced deviations in CCSs, with up to 59% β-sheet features in the amide I band for the largest of the four different pentameric species (5/3) of YVEALL (filled circles). However, a clear linear correlation between deviation in CCS and β-sheet content does not exist, because the intrinsic structural heterogeneity of the system probably contributes significantly to the scatter in this plot. Nevertheless, the data indicate a positive relationship between the relative cross-section and the relative amount of ordered β-sheet structure, and therefore support recent IMS–MS approaches in which such a correlation was suggested[20,22–26].

Conclusions

Combining IMS–MS and infrared spectroscopy has enabled us to measure directly the onset of β-sheet-structure formation in isolated, early soluble oligomers of the insulin β-chain fragment VEALYL, which was previously shown to form β-sheet-rich amyloid fibrils and microcrystals[15]. In addition, the critical transition from a compact and unordered to an extended β-sheet structure was monitored for highly polymorphic pentamers of the amyloidogenic VEALYL sequence variant YVEALL. Compact YVEALL pentamers were shown to adopt predominantly turn-like or unfolded structures and a considerably increased content of β-sheets was observed for the more-extended analogues. Further support for this structural assignment was found in amide III and side-chain vibrations, which follow the evolution of β-sheet-characteristic amide I features and strongly suggest that the peptide assemblies consist of repeating β-sheets. Taken together, the data represent the first spectroscopic study that successfully identifies specific pre-fibrillar oligomer states involved in the critical transition from an unordered to a β-sheet-rich structure. For the systems investigated here, oligomers that consist of as little as 4–9 peptide strands were found to exhibit a considerable fraction of β-sheets.

Furthermore, the results presented here demonstrate that there is a positive correlation between a large CCS that deviates from the isotropic growth model and the presence of β-sheet structures. This correlation greatly strengthens the interpretation given in recent IMS–MS studies of amyloid systems[20,22–26] and demonstrates how infrared-spectroscopy combined with IMS–MS can be of great use in this field of research. These combined techniques offer new possibilities to explore the secondary structures of soluble pre-fibrillar oligomers, which will be greatly beneficial for developing effective strategies to manipulate or hinder the amyloid-assembly process[22,26–28] and may ultimately help to understand the molecular basis of amyloid diseases.

Methods

Brief details are given here, with more detailed experimental methods including solid-phase peptide syntheses, TEM measurements, ultraviolet spectroscopy, solid and solution FTIR and IRMPD spectroscopy, IMS–MS and data fitting described in Supplementary Information. Mass spectra, arrival time distributions, CCSs and IRMPD spectra of all the hexapeptide oligomers are also given.

Materials. All the solvents were purchased from Sigma-Aldrich and used without further purification. The three reported hexapeptides were synthesized using standard Fmoc (9-fluorenyl-methoxycarbonyl) solid-phase peptide synthesis (SPPS)[39]. SPPS was carried out on a fully automated peptide synthesizer (Activo-P11 (Activotec) or Syro XP-1 (Multi-Syn Tech)). The synthesized peptides were further purified by reverse-phase HPLC (details given in Supplementary Fig. 1 and Supplementary Tables 1 and 2). Sample solutions were prepared by dissolving peptides in water/methanol (1/1, v/v) to a final concentration of 2 mM. Instead of pure water, water/methanol was chosen to ensure stable spray conditions and to reduce possible nonspecific aggregation, which can occur at this high sample concentration. The pH of each sample solution was determined to be ~3.0 by using a WTW pH526 pH meter equipped with an InLab Micro electrode (Mettler Toledo).

TEM. Aliquots of the peptide sample solutions (2 mM, pH ~3) were deposited onto a carbon-coated Cu grid by drop casting. After being dried in ambient air, they were put into an FEI aberration-corrected Titan 80–300 microscope operated at 300 kV from which the TEM micrographs were obtained.

Solid-state FTIR spectroscopy. Peptide solutions (2 mM) were incubated under stirring at 37 °C for 24 hours. Subsequently, the formed precipitates were isolated from solution by centrifugation at 12,000*g* for ten minutes. The supernatants were transfused and the precipitates were freeze-dried. The background-corrected FTIR spectra (650–4,000 cm^{-1}) of the precipitates were measured using a JASCO FT/IR-4100 spectrometer (JASCO) in the transmission mode. Solid samples for the non-fibril forming sequence VELYAL were prepared by quick-freezing the incubated sample solution and further freeze-drying. Solid FTIR spectra of freshly dissolved sample solutions were prepared as described for the incubated VELYAL sample solution.

IMS–MS coupled to IRMPD spectroscopy. Peptide solutions were diluted further to the desired concentration (0.15–2 mM), loaded into Pd/Pt-coated nanoelectrospray ionization emitters and electrosprayed on a home-built drift-tube

ion-mobility mass spectrometer[40–42] fashioned after an IMS–MS instrument previously designed and built at University of California Santa Barbara[43]. Ions were transferred and stored in an ion funnel and pulsed into the drift tube, where they travelled under the influence of a weak electric field (10–20 V cm^{-1}) through helium buffer gas (~4 mbar) and were separated according to their drift time. After the ion-mobility separation, a particular aggregation state was isolated by *m*/*z* selection using a quadrupole mass filter and its ATD was recorded. The CCS was calculated from the measured arrival time (see Supplementary Information for the details). Ion-mobility and *m*/*z*-selective IRMPD spectroscopy was performed by selecting a narrow fraction of the drift-time distribution (100 μs) prior to *m*/*z* selection and subsequent irradiation of the ions with infrared radiation provided by the FHI-FEL[34]. The absorption of multiple photons leads to fragmentation and emerging fragments are detected by a time-of-flight mass analyser. The final IRMPD spectra are composed by plotting the fragmentation yield as a function of the infrared wavenumber (see Supplementary Figs 2 and 3 for details).

Received 26 November 2015; accepted 10 August 2016; published online 26 September 2016

References

1. Caughey, B. & Lansbury, P. T. Protofibrils, pores, fibrils, and neurodegeneration: separating the responsible protein aggregates from the innocent bystanders. *Annu. Rev. Neurosci.* **26,** 267–298 (2003).
2. Dobson, C. M. Protein folding and misfolding. *Nature* **426,** 884–890 (2003).
3. Selkoe, D. J. Folding proteins in fatal ways. *Nature* **426,** 900–904 (2003).
4. Walsh, D. M. *et al.* Naturally secreted oligomers of amyloid β protein potently inhibit hippocampal long-term potentiation *in vivo*. *Nature* **416,** 535–539 (2002).
5. Goedert, M. & Spillantini, M. G. A century of Alzheimer's disease. *Science* **314,** 777–781 (2006).
6. Lesné, S. *et al.* A specific amyloid-β protein assembly in the brain impairs memory. *Nature* **440,** 352–357 (2006).
7. Winner, B. *et al. In vivo* demonstration that α-synuclein oligomers are toxic. *Proc. Natl Acad. Sci. USA* **108,** 4194–4199 (2011).
8. Lin, C.-Y. *et al.* Toxic human islet amyloid polypeptide (h-IAPP) oligomers are intracellular, and vaccination to induce anti-toxic oligomer antibodies does not prevent h-IAPP-induced β-cell apoptosis in h-IAPP transgenic mice. *Diabetes* **56,** 1324–1332 (2007).
9. Gurlo, T. *et al.* Evidence for proteotoxicity in β cells in type 2 diabetes: toxic islet amyloid polypeptide oligomers form intracellularly in the secretory pathway. *Am. J. Pathol.* **176,** 861–869 (2010).
10. Chiti, F. & Dobson, C. M. Protein misfolding, functional amyloid, and human disease. *Annu. Rev. Biochem.* **75,** 333–366 (2006).
11. Ivanova, M. I., Sievers, S. A., Sawaya, M. R., Wall, J. S. & Eisenberg, D. Molecular basis for insulin fibril assembly. *Proc. Natl Acad. Sci. USA* **106,** 18990–18995 (2009).
12. Nelson, R. *et al.* Structure of the cross-β spine of amyloid-like fibrils. *Nature* **435,** 773–778 (2005).
13. Stromer, T. & Serpell, L. C. Structure and morphology of the Alzheimer's amyloid fibril. *Microsc. Res. Tech.* **67,** 210–217 (2005).
14. Sawaya, M. R. *et al.* Atomic structures of amyloid cross-β spines reveal varied steric zippers. *Nature* **447,** 453–457 (2007).
15. Matthes, D. *et al.* Spontaneous aggregation of the insulin-derived steric zipper peptide VEALYL results in different aggregation forms with common features. *J. Mol. Biol.* **426,** 362–376 (2014).
16. Cerf, E. *et al.* Antiparallel β-sheet: a signature structure of the oligomeric amyloid β-peptide. *Biochem. J.* **421,** 415–423 (2009).
17. Celej, M. S. *et al.* Toxic prefibrillar α-synuclein amyloid oligomers adopt a distinctive antiparallel β-sheet structure. *Biochem. J.* **443,** 719–726 (2012).
18. Buchanan, L. E. *et al.* Mechanism of IAPP amyloid fibril formation involves an intermediate with a transient β-sheet. *Proc. Natl Acad. Sci. USA* **110,** 19285–19290 (2013).
19. Bernstein, S. L. *et al.* Amyloid-β protein oligomerization and the importance of tetramers and dodecamers in the aetiology of Alzheimer's disease. *Nat. Chem.* **1,** 326–331 (2009).
20. Bleiholder, C., Dupuis, N. F., Wyttenbach, T. & Bowers, M. T. Ion mobility-mass spectrometry reveals a conformational conversion from random assembly to β-sheet in amyloid fibril formation. *Nat. Chem.* **3,** 172–177 (2011).
21. Dupuis, N. F., Wu, C., Shea, J.-E. & Bowers, M. T. The amyloid formation mechanism in human IAPP: dimers have β-strand monomer–monomer interfaces. *J. Am. Chem. Soc.* **133,** 7240–7243 (2011).
22. Bleiholder, C. *et al.* Ion mobility spectrometry reveals the mechanism of amyloid formation of Aβ(25–35) and its modulation by inhibitors at the molecular level: epigallocatechin gallate and scyllo-inositol. *J. Am. Chem. Soc.* **135,** 16926–16937 (2013).
23. Do, T. D. *et al.* Effects of pH and charge state on peptide assembly: the YVIFL model system. *J. Phys. Chem. B* **117,** 10759–10768 (2013).
24. Do, T. D. *et al.* Interactions between amyloid-β and tau fragments promote aberrant aggregates: implications for amyloid toxicity. *J. Phys. Chem. B* **118,** 11220–11230 (2014).
25. Do, T. D. *et al.* Factors that drive peptide assembly from native to amyloid structures: experimental and theoretical analysis of [leu-5]-enkephalin mutants. *J. Phys. Chem. B* **118,** 7247–7256 (2014).
26. Young, L. M., Cao, P., Raleigh, D. P., Ashcroft, A. E. & Radford, S. E. Ion mobility spectrometry–mass spectrometry defines the oligomeric intermediates in amylin amyloid formation and the mode of action of inhibitors. *J. Am. Chem. Soc.* **136,** 660–670 (2014).
27. Young, L. M. *et al.* Screening and classifying small-molecule inhibitors of amyloid formation using ion mobility spectrometry–mass spectrometry. *Nat. Chem.* **7,** 73–81 (2015).
28. Zheng, X. Y. *et al.* Amyloid β-protein assembly: the effect of molecular tweezers CLR01 and CLR03. *J. Phys. Chem. B* **119,** 4831–4841 (2015).
29. Jackson, M. & Mantsch, H. H. The use and misuse of FTIR spectroscopy in the determination of protein structure. *Crit. Rev. Biochem. Mol. Biol.* **30,** 95–120 (1995).
30. Barth, A. Infrared spectroscopy of proteins. *Biochim. Biophys. Acta* **1767,** 1073–1101 (2007).
31. Oomens, J., Sartakov, B. G., Meijer, G. & von Helden, G. Gas-phase infrared multiple photon dissociation spectroscopy of mass-selected molecular ions. *Int. J. Mass Spectrom.* **254,** 1–19 (2006).
32. Papadopoulos, G., Svendsen, A., Boyarkin, O. V. & Rizzo, T. R. Spectroscopy of mobility-selected biomolecular ions. *Faraday Discuss.* **150,** 243–255 (2010).
33. Knowles, T. P. J. *et al.* An analytical solution to the kinetics of breakable filament assembly. *Science* **326,** 1533–1537 (2009).
34. Schöllkopf, W. *et al.* The new IR and THz FEL facility at the Fritz Haber Institute in Berlin, *Advances in X-ray Free-Electron Lasers Instrumentation III* (ed. Briedon, S.G.) (*Proc. of SPIE* Vol. 9512, SPIE, 2015).
35. Cai, S. & Singh, B. R. A distinct utility of the amide III infrared band for secondary structure estimation of aqueous protein solutions using partial least squares methods. *Biochemistry* **43,** 2541–2549 (2004).
36. Bleiholder, C., Wyttenbach, T. & Bowers, M. T. A novel projection approximation algorithm for the fast and accurate computation of molecular collision cross sections. (I) Method. *Int. J. Mass Spectrom.* **308,** 1–10 (2011).
37. Wyttenbach, T., Bleiholder, C. & Bowers, M. T. Factors contributing to the collision cross section of polyatomic ions in the kilodalton to gigadalton range: application to ion mobility measurements. *Anal. Chem.* **85,** 2191–2199 (2013).
38. Marklund, E. G., Degiacomi, M. T., Baldwin, A. J. & Benesch, J. L. P. Collision cross sections for structural proteomics. *Structure* **23,** 1–9 (2015).
39. Atherton, E. & Sheppard, R. C. *Solid Phase Peptide Synthesis: A Practical Approach* (Oxford Univ. Press, 1989).
40. Warnke, S., von Helden, G. & Pagel, K. Protein structure in the gas phase: the influence of side-chain microsolvation. *J. Am. Chem. Soc.* **135,** 1177–1180 (2013).
41. Warnke, S., Baldauf, C., Bowers, M. T., Pagel, K. & von Helden, G. Photodissociation of conformer-selected ubiquitin ions reveals site-specific *cis*/*trans* isomerization of proline peptide bonds. *J. Am. Chem. Soc.* **136,** 10308–10314 (2014).
42. Warnke, S. *et al.* Protomers of benzocaine: solvent and permittivity dependence. *J. Am. Chem. Soc.* **137,** 4236–4242 (2015).
43. Kemper, P. R., Dupuis, N. F. & Bowers, M. T. A new, higher resolution, ion mobility mass spectrometer. *Int. J. Mass Spectrom.* **287,** 46–57 (2009).

Acknowledgements

The authors thank S. Huhmann for the help during synthesis, L. Urner for fruitful discussion and R. Schlögl for proofreading the manuscript. B. Koksch and M. Villinger are gratefully acknowledged for providing the peptide synthesis facilities and EM infrastructure. M.T.B. acknowledges the Alexander von Humboldt-Foundation and the National Science Foundation for support under grant CHE-1301032.

Author contributions

J.S., W.H., M.T.B., G.v.H. and K.P. conceived and designed the experiments; J.S., W.H. and S.W. performed the experiments: X.H., S.G. and W.S. supported the experiments; J.S. and W.H. analysed data; all the authors co-wrote the paper. J.S. and W.H. contributed equally to this work.

Additional information

Supplementary information is available in the online version of the paper. Reprints and permissions information is available online at www.nature.com/reprints. Correspondence and requests for materials should be addressed to G.v.H. and K.P.

Competing financial interests

The authors declare no competing financial interests.